Magnetization damping in noncollinear spin valves with antiferromagnetic interlayer couplings

Takahiro Chiba,[1,*] Gerrit E. W. Bauer,[1,2,3] and Saburo Takahashi[1]
[1]*Institute for Materials Research, Tohoku University, Sendai 980-8577, Japan*
[2]*WPI-AIMR, Tohoku University, Sendai 980-8577, Japan*
[3]*Kavli Institute of NanoScience, Delft University of Technology, Lorentzweg 1, 2628 CJ Delft, The Netherlands*
(Received 23 April 2015; published 5 August 2015)

We study the magnetic damping in the simplest of synthetic antiferromagnets, i.e., antiferromagnetically exchange-coupled spin valves, in the presence of applied magnetic fields that enforce noncolliear magnetic configurations. We formulate the dynamic exchange of spin currents in a noncollinear texture based on the spin-diffusion theory with quantum mechanical boundary conditions at the ferrromagnet/normal-metal interfaces and derive the Landau-Lifshitz-Gilbert equations coupled by the interlayer static and dynamic exchange interactions. We predict noncollinearity-induced additional damping that is modulated by an applied magnetic field. We compare theoretical results with published experiments.

DOI: 10.1103/PhysRevB.92.054407 PACS number(s): 72.25.Mk, 75.40.Gb, 75.70.Cn, 76.50.+g

I. INTRODUCTION

Antiferromagnets (AFMs) boast many of the functionalities of ferromagnets (FMs) that are useful in spintronic circuits and devices: Anisotropic magnetoresistance (AMR) [1], tunneling anisotropic magnetoresistance (TAMR) [2], current-induced spin-transfer torque [3–8], and spin-current transmission [9–11] have all been found in or with AFMs. This is of interest because AFMs have additional features potentially attractive for applications. In AFMs, the total magnetic moment is (almost) completely compensated on an atomic length scale. The AFM order parameter is, hence, robust against perturbations such as external magnetic fields and does not generate stray fields. A spintronic technology based on AFM elements is therefore very attractive [12,13]. Drawbacks are the difficulty to *control* AFMs by magnetic fields and much higher (THz) resonance frequencies [14–16], which are difficult to match with conventional electronic circuits. Manmade magnetic multilayers in which the layer magnetizations in the ground state are ordered in an antiparallel fashion [17], i.e., so-called synthetic antiferromagnets, do not suffer from this drawback and have therefore been a fruitful laboratory to study and modulate antiferromagnetic couplings and its consequences [18] as well as to find applications such as magnetic field sensors [19]. Transport in these multilayers including the giant magnetoresistance (GMR) [20,21] are now well understood in terms of spin- and charge-diffusive transport. Current-induced magnetization switching in F|N|F spin valves and tunnel junctions [22] has been a game changer for devices such as magnetic random access memories (MRAM) [23]. A key parameter of magnetization dynamics is the magnetic damping; a small damping lowers the threshold of current-driven magnetization switching [24], whereas a large damping suppresses "ringing" of the switched magnetization [25].

Magnetization dynamics in multilayers generates "spin pumping," i.e., spin-current injection from the ferromagnet into metallic contacts. It is associated with a loss of angular momentum and an additional interface-related magnetization damping [26,27]. In spin valves, the additional damping is suppressed when the two magnetizations precess in phase, while it is enhanced for a phase difference of π (out of phase) [27–30]. This phenomenon is explained in terms of a "dynamic exchange interaction," i.e., the mutual exchange of nonequilibrium spin currents, which should be distinguished from (but coexists with) the oscillating equilibrium exchange coupling mediated by the Ruderman-Kittel-Kasuya-Yosida (RKKY) interaction. The latter equilibrium coupling is suppressed when the spacer thickness exceeds the elastic mean free path [31,32], while the dynamic coupling is effective on the scale of the usually much larger spin-flip diffusion length.

Antiparallel spin valves provide a unique opportunity to study and control the dynamic exchange interaction between ferromagnets through a metallic interlayer for tunable magnetic configurations [33–36]. An originally antiparallel configuration is forced by relatively weak external magnetic fields into a noncollinear configuration with a ferromagnetic component. Ferromagnetic resonance (FMR) and Brillouin light scattering (BLS) are two useful experimental methods to investigate the nature and magnitude of exchange interactions and magnetic damping in multilayers [37]. Both methods observe two resonances, i.e., acoustic (A) and optical (O) modes, which are characterized by their frequencies and linewidths [38,39].

Timopheev *et al.* [40] observed an effect of the interlayer RKKY coupling on the FMR and found the linewidth to be affected by the dynamic exchange coupling in spin valves with one layer fixed by the exchange bias of an inert AFM substrate. They measured the FMR spectrum of the free layer by tuning the interlayer coupling (thickness) and reported a broadening of the linewidth by the dynamic exchange interaction. Taniguchi *et al.* addressed theoretically the enhancement of the Gilbert damping constant due to spin pumping in noncollinear F|N|F trilayer systems, in which one of the magnetizations is excited by FMR, while the other is off resonant, but adopts a role as spin sink [41]. The dynamics of coupled spin valves in which both layer magnetizations are free to move has been computed by one of us [29], by Kim *et al.* [42], and by Skarsvåg *et al.* [35,43], but only for collinear (parallel and antiparallel) configurations. Current-induced high-frequency oscillations

*t.chiba@imr.tohoku.ac.jp

without applied magnetic field in ferromagnetically coupled spin valves have been predicted [44].

In the present paper, we model the magnetization dynamics of the simplest of synthetic antiferromagnets, i.e., the antiferromagnetically exchange-coupled spin valve in which the (in-plane) ground-state magnetizations are for certain spacer thicknesses ordered in an antiparallel fashion by the RKKY interlayer coupling [45]. We focus on the coupled magnetization modes in symmetric spin valves in which, in contrast to previous studies, both magnetizations are free to move. We include static magnetic fields in the film plane that deform the antiparallel configuration into a canted one. Microwaves with longitudinal and transverse polarizations with respect to an external magnetic field then excite A and O resonance modes, respectively [31,46–50]. We develop the theory for magnetization dynamics and damping based on the Landau-Lifshitz-Gilbert equation with mutual pumping of spin currents and spin-transfer torques based on the spin-diffusion model with quantum mechanical boundary conditions [27,51,52]. We confirm [28,43] that the additional damping of the O modes is larger than that of the A modes. We report that a noncollinear magnetization configuration induces additional damping torques. The external magnetic field strongly affects the dynamics by modulating the phase of the dynamic exchange interaction. We compute FMR linewidths as a function of applied magnetic fields and find good agreement with experimental FMR spectra on spin valves [31,32]. The dynamics of magnetic multilayers as measured by ac spin-transfer torque excitation [30] reveals a relative broadening of the O-mode linewidths that is well reproduced by our spin-valve model.

In Sec. II, we present our model for noncollinear spin valves based on spin-diffusion theory with quantum mechanical boundary conditions. In Sec. III, we consider the magnetization dynamics in antiferromagnetically coupled noncollinear spin valves, as shown in Fig. 1(b). We derive the linearized magnetization dynamics, resonance frequencies, and lifetimes of the acoustic and optical resonance modes in Sec. IV. We discuss the role of dynamic spin torques on noncollinear magnetization configurations in relation to external magnetic field dependence of the linewidth. In Sec. V, we compare the calculated microwave absorption and linewidth with published experiments. We summarize the results and end with the conclusions in Sec. VI.

II. SPIN-DIFFUSION TRANSPORT MODEL

We consider F1|N|F2 spin valves, as shown in Fig. 1(a), in which the magnetizations $\mathbf{M}_j$ of the ferromagnets Fj ($j = 1,2$) are coupled by an antiparallel interlayer exchange interaction and tilted towards the direction of an external magnetic field. Applied microwaves with transverse polarizations with respect to an external magnetic field cause dynamics and, via spin pumping, spin currents and accumulations in the normal-metal (NM) spacer. The longitudinal component of the spin accumulation diffuses into and generates spin accumulations in F that we show to be small later, but disregard initially. Let us denote the pumped spin current $\mathbf{J}^{\mathrm{P}}_j$, while $\mathbf{J}^{\mathrm{B}}_j$ is the diffusion (backflow) spin-current density induced by a

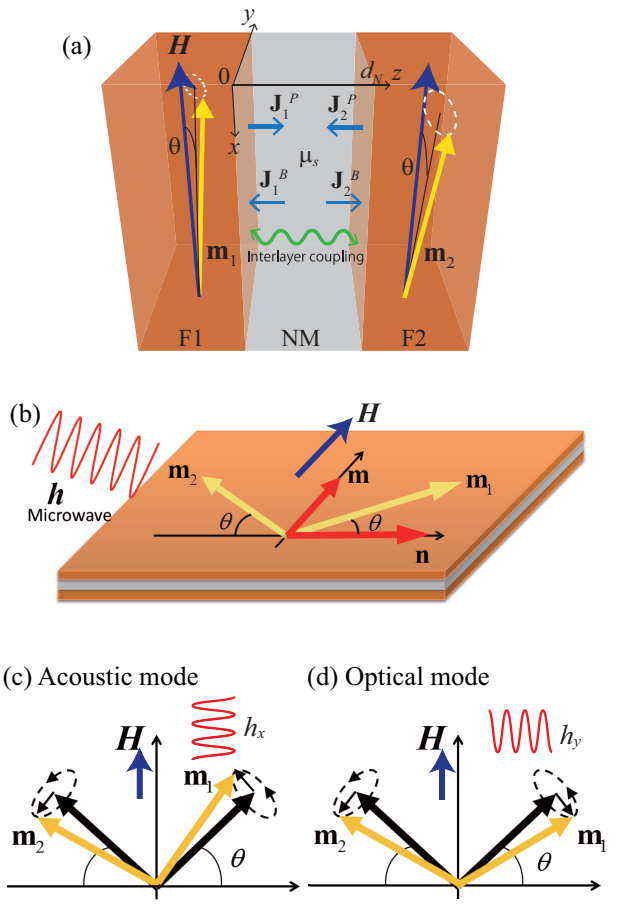

FIG. 1. (Color online) (a) Sketch of the sample with interlayer exchange couplings illustrating the spin pumping and backflow currents. (b) Magnetic resonance in an antiferromagnetically exchange-coupled spin valve with a normal-metal (NM) film sandwiched by two ferromagnets (F1, F2) subject to a microwave magnetic field $\mathbf{h}$. The magnetization vectors ($\mathbf{m}_1$, $\mathbf{m}_2$) are tilted by an angle θ in a static in-plane magnetic field $\mathbf{H}$ applied along the y axis. The vectors $\mathbf{m}$ and $\mathbf{n}$ represent the sum and difference of the two layer magnetizations, respectively. (c),(d) Precession-phase relations for the acoustic and optical modes.

spin accumulation $\boldsymbol{\mu}_{sj}$ in NM, both at the interface Fj, with [27,53]

$$\mathbf{J}^{\mathrm{P}}_j = \frac{G_r}{e}\mathbf{m}_j \times \hbar\partial_t \mathbf{m}_j, \tag{1a}$$

$$\mathbf{J}^{\mathrm{B}}_j = \frac{G_r}{e}[(\mathbf{m}_j \cdot \boldsymbol{\mu}_{sj})\mathbf{m}_j - \boldsymbol{\mu}_{sj}], \tag{1b}$$

where $\mathbf{m}_j = \mathbf{M}_j/|\mathbf{M}_j|$ is the unit vector along the magnetic moment of Fj ($j = 1,2$). The spin current through a FM|NM interface is governed by the complex spin-mixing conductance (per unit area of the interface), $G^{\uparrow\downarrow} = G_r + iG_i$ [27]. The real component G_r parameterized one vector component of the transverse spin currents pumped and absorbed by the ferromagnets. The imaginary part G_i can be interpreted as an effective exchange field between magnetization and spin accumulation, which in the absence of spin-orbit interaction is usually much smaller than the real part, for conducting as well as insulting magnets [54].

The diffusion spin-current density in NM reads

$$\mathbf{J}_{s,z}(z) = -\frac{\sigma}{2e}\partial_z \boldsymbol{\mu}_s(z), \tag{2}$$

where $\sigma = \rho^{-1}$ is the electrical conductivity and $\boldsymbol{\mu}_s(z) = \boldsymbol{A}e^{-z/\lambda} + \boldsymbol{B}e^{z/\lambda}$ is the spin accumulation vector that is a solution of the spin-diffusion equation $\partial_z^2\boldsymbol{\mu}_s = \boldsymbol{\mu}_s/\lambda^2$, where $\lambda = \sqrt{D\tau_{\rm sf}}$ is the spin-diffusion length, D is the diffusion constant, and $\tau_{\rm sf}$ is the spin-flip relaxation time. The vectors $\boldsymbol{A}$ and $\boldsymbol{B}$ are determined by the boundary conditions at the F1|NM ($z = 0$) and F2|NM ($z = d_{\rm N}$) interfaces: $\mathbf{J}_{s,z}(0) = \mathbf{J}_1^{\rm P} + \mathbf{J}_1^{\rm B} \equiv \mathbf{J}_{s1}$ and $\mathbf{J}_{s,z}(d_{\rm N}) = -\mathbf{J}_2^{\rm P} - \mathbf{J}_2^{\rm B} \equiv -\mathbf{J}_{s2}$. The resulting spin accumulation in N reads

$$\boldsymbol{\mu}_s(z) = \frac{2e\lambda\rho}{\sinh\left(\frac{d_{\rm N}}{\lambda}\right)}\left[\mathbf{J}_{s1}\cosh\left(\frac{z-d_{\rm N}}{\lambda}\right) + \mathbf{J}_{s2}\cosh\left(\frac{z}{\lambda}\right)\right], \tag{3}$$

with interface spin currents

$$\mathbf{J}_{s1} = \frac{\eta S}{1-\eta^2}\left[\delta\mathbf{J}_1^{\rm P} + \frac{\eta^2\left(\mathbf{m}_2\cdot\delta\mathbf{J}_1^{\rm P}\right)}{1-\eta^2(\mathbf{m}_1\cdot\mathbf{m}_2)^2}\mathbf{m}_1\times(\mathbf{m}_1\times\mathbf{m}_2)\right], \tag{4a}$$

$$\mathbf{J}_{s2} = -\frac{\eta S}{1-\eta^2}\left[\delta\mathbf{J}_2^{\rm P} + \frac{\eta^2\left(\mathbf{m}_1\cdot\delta\mathbf{J}_2^{\rm P}\right)}{1-\eta^2(\mathbf{m}_1\cdot\mathbf{m}_2)^2}\mathbf{m}_2\times(\mathbf{m}_2\times\mathbf{m}_1)\right]. \tag{4b}$$

Here,

$$\delta\mathbf{J}_1^{\rm P} = \mathbf{J}_1^{\rm P} + \eta\mathbf{m}_1\times\left(\mathbf{m}_1\times\mathbf{J}_2^{\rm P}\right), \tag{5a}$$

$$\delta\mathbf{J}_2^{\rm P} = \mathbf{J}_2^{\rm P} + \eta\mathbf{m}_2\times\left(\mathbf{m}_2\times\mathbf{J}_1^{\rm P}\right), \tag{5b}$$

$S = \sinh(d_{\rm N}/\lambda)/g_r$ and $\eta = g_r/[\sinh(d_{\rm N}/\lambda) + g_r\cosh(d_{\rm N}/\lambda)]$ are the efficiency of the backflow spin currents, and $g_r = 2\lambda\rho G_r$ is dimensionless. The first terms in Eqs. (4a) and (4b) represent the mutual pumping of spin currents, while the second terms may be interpreted as a spin current induced by the noncollinear magnetization configuration, including the backflow from the NM interlayer.

III. MAGNETIZATION DYNAMICS WITH DYNAMIC SPIN TORQUES

We consider the magnetic resonance in the noncollinear spin valve shown in Fig. 1. The magnetization dynamics are described by the Landau-Lifshitz-Gilbert (LLG) equation,

$$\partial_t\mathbf{m}_1 = -\gamma\mathbf{m}_1\times\mathbf{H}_{\rm eff1} + \alpha_0\mathbf{m}_1\times\partial_t\mathbf{m}_1 + \boldsymbol{\tau}_1, \tag{6a}$$

$$\partial_t\mathbf{m}_2 = -\gamma\mathbf{m}_2\times\mathbf{H}_{\rm eff2} + \alpha_0\mathbf{m}_2\times\partial_t\mathbf{m}_2 - \boldsymbol{\tau}_2. \tag{6b}$$

The first term in Eqs. (6a) and (6b) represents the torque induced by the effective magnetic field,

$$\mathbf{H}_{\rm eff1(2)} = \mathbf{H} + \mathbf{h}(t) - 4\pi M_s m_{1(2)z}\hat{\mathbf{z}} + \frac{J_{\rm ex}}{M_s d_{\rm F}}\mathbf{m}_{2(1)}, \tag{7}$$

which consists of an in-plane applied magnetic field $\mathbf{H}$, a microwave field $\mathbf{h}(t)$, and the demagnetization field $-4\pi M_s m_{1(2)z}\hat{\mathbf{z}}$ with saturation magnetization M_s. The interlayer exchange field is $J_{\rm ex}/(M_s d_{\rm F})\mathbf{m}_{2(1)}$ with areal density of the interlayer exchange energy $J_{\rm ex} < 0$ (for antiferromagnetic coupling) and F layer thickness $d_{\rm F}$. The second term is the Gilbert damping torque that governs the relaxation characterized by α_{0i} towards an equilibrium direction. The third term, $\boldsymbol{\tau}_{1(2)} = \gamma\hbar/(2eM_s d_{\rm F})\mathbf{J}_{s1(2)}$, is the spin-transfer torque induced by the absorption of the transverse spin currents of Eqs. (4a) and (4b), and γ and α_0 are the gyromagnetic ratio and the Gilbert damping constant of the isolated ferromagnetic films, respectively. Some technical details of the coupled LLG equations are discussed in the Appendix. Introducing the total magnetization direction $\mathbf{m} = (\mathbf{m}_1 + \mathbf{m}_2)/2$ and the difference vector $\mathbf{n} = (\mathbf{m}_1 - \mathbf{m}_2)/2$, the LLG equations can be written

$$\begin{aligned}\partial_t\mathbf{m} = {}& -\gamma\mathbf{m}\times(\mathbf{H}+\mathbf{h}) + 2\pi\gamma M_s(m_z\mathbf{m} + n_z\mathbf{n})\times\hat{\mathbf{z}} \\ & + \alpha_0(\mathbf{m}\times\partial_t\mathbf{m} + \mathbf{n}\times\partial_t\mathbf{n}) + \boldsymbol{\tau}_m,\end{aligned} \tag{8a}$$

$$\begin{aligned}\partial_t\mathbf{n} = {}& -\gamma\mathbf{n}\times\left(\mathbf{H}+\mathbf{h}+\frac{J_{\rm ex}}{M_s d_{\rm F}}\mathbf{m}\right) \\ & + 2\pi\gamma M_s(n_z\mathbf{m} + m_z\mathbf{n})\times\hat{\mathbf{z}} \\ & + \alpha_0(\mathbf{m}\times\partial_t\mathbf{n} + \mathbf{n}\times\partial_t\mathbf{m}) + \boldsymbol{\tau}_n,\end{aligned} \tag{8b}$$

where the spin-transfer torques $\boldsymbol{\tau}_m = (\boldsymbol{\tau}_1 + \boldsymbol{\tau}_2)/2$ and $\boldsymbol{\tau}_n = (\boldsymbol{\tau}_1 - \boldsymbol{\tau}_2)/2$ become

$$\begin{aligned}\boldsymbol{\tau}_m/\alpha_m = {}& \mathbf{m}\times\partial_t\mathbf{m} + \mathbf{n}\times\partial_t\mathbf{n} \\ & + 2\eta\frac{\mathbf{m}\cdot(\mathbf{n}\times\partial_t\mathbf{n})}{1-\eta C}\mathbf{m} + 2\eta\frac{\mathbf{n}\cdot(\mathbf{m}\times\partial_t\mathbf{m})}{1+\eta C}\mathbf{n},\end{aligned} \tag{9a}$$

$$\begin{aligned}\boldsymbol{\tau}_n/\alpha_n = {}& \mathbf{m}\times\partial_t\mathbf{n} + \mathbf{n}\times\partial_t\mathbf{m} \\ & - 2\eta\frac{\mathbf{m}\cdot(\mathbf{n}\times\partial_t\mathbf{m})}{1+\eta C}\mathbf{m} - 2\eta\frac{\mathbf{n}\cdot(\mathbf{m}\times\partial_t\mathbf{n})}{1-\eta C}\mathbf{n},\end{aligned} \tag{9b}$$

and $C = \mathbf{m}^2 - \mathbf{n}^2$, while

$$\alpha_m = \frac{\alpha_1 g_r}{1 + g_r\coth(d_{\rm N}/2\lambda)}, \tag{10a}$$

$$\alpha_n = \frac{\alpha_1 g_r}{1 + g_r\tanh(d_{\rm N}/2\lambda)}, \tag{10b}$$

with $\alpha_1 = \gamma\hbar^2/(4e^2\lambda\rho M_s d_{\rm F})$.

IV. CALCULATIONS AND RESULTS

We consider the magnetization dynamics excited by linearly polarized microwaves with a frequency ω and in-plane magnetic field $\mathbf{h}(t) = (h_x, h_y, 0)e^{i\omega t}$ that is much smaller than the saturation magnetization. For small-angle magnetization precession, the total magnetization and difference vector may be separated into a static equilibrium and a dynamic component as $\mathbf{m} = \mathbf{m}_0 + \delta\mathbf{m}$ and $\mathbf{n} = \mathbf{n}_0 + \delta\mathbf{n}$, respectively, where $\mathbf{m}_0 = (0, \sin\theta, 0)$, $\mathbf{n}_0 = (\cos\theta, 0, 0)$, $C = -\cos 2\theta$, and $\boldsymbol{s} = -\hat{\mathbf{z}}\sin 2\theta$. The equilibrium (zero torque) conditions $\mathbf{m}_0\times\mathbf{H} = 0$ and $\mathbf{n}_0\times[\mathbf{H} + J_{\rm ex}/(M_s d_{\rm F})\mathbf{m}_0] = 0$ lead to the relation

$$\sin\theta = H/H_s, \tag{11}$$

where $H_s = -J_{\rm ex}/(M_s d_{\rm F}) = |J_{\rm ex}|/(M_s d_{\rm F})$ is the saturation field. The LLG equations read

$$\begin{aligned}\partial_t \delta\mathbf{m} &= -\gamma\delta\mathbf{m}\times\mathbf{H} - \gamma\mathbf{m}_0\times\mathbf{h}\\ &\quad + 2\pi\gamma M_s(\delta m_z\mathbf{m}_0 + \delta n_z\mathbf{n}_0)\times\hat{\mathbf{z}}\\ &\quad + \alpha_0(\mathbf{m}_0\times\partial_t\delta\mathbf{m} + \mathbf{n}_0\times\partial_t\delta\mathbf{n}) + \delta\boldsymbol{\tau}_{\rm m}, \quad (12a)\\ \partial_t \delta\mathbf{n} &= -\gamma\delta\mathbf{n}\times\mathbf{H} - \gamma\mathbf{n}_0\times\mathbf{h}\\ &\quad + 2\pi\gamma M_s(\delta n_z\mathbf{m}_0 + \delta m_z\mathbf{n}_0)\times\hat{\mathbf{z}}\\ &\quad - \gamma H_s(\mathbf{m}_0\times\delta\mathbf{n} - \mathbf{n}_0\times\delta\mathbf{m})\\ &\quad + \alpha_0(\mathbf{m}_0\times\partial_t\delta\mathbf{n} + \mathbf{n}_0\times\partial_t\delta\mathbf{m}) + \delta\boldsymbol{\tau}_{\rm n}, \quad (12b)\end{aligned}$$

with linearized spin-transfer torques

$$\begin{aligned}\delta\boldsymbol{\tau}_m/\alpha_m &= \mathbf{m}_0\times\partial_t\delta\mathbf{m} + \mathbf{n}_0\times\partial_t\delta\mathbf{n}\\ &\quad - \frac{\eta\sin 2\theta}{1+\eta\cos 2\theta}\partial_t\delta n_z\mathbf{m}_0 + \frac{\eta\sin 2\theta}{1-\eta\cos 2\theta}\partial_t\delta m_z\mathbf{n}_0, \quad (13a)\\ \delta\boldsymbol{\tau}_n/\alpha_n &= \mathbf{m}_0\times\partial_t\delta\mathbf{n} + \mathbf{n}_0\times\partial_t\delta\mathbf{m}\\ &\quad + \frac{\eta\sin 2\theta}{1-\eta\cos 2\theta}\delta m_z\mathbf{m}_0 - \frac{\eta\sin 2\theta}{1+\eta\cos 2\theta}\delta n_z\mathbf{n}_0. \quad (13b)\end{aligned}$$

To leading order in the small precessing components $\delta\mathbf{m}$ and $\delta\mathbf{n}$, the LLG equations in frequency space become

$$\delta m_x = \gamma h_x \frac{\gamma(H_s+4\pi M_s) + i\omega\left[\alpha_0 + \frac{\alpha_m(1+\eta)}{1-\eta\cos 2\theta}\right]}{\omega^2 - \omega_{\rm A}^2 - i\Delta_{\rm A}\omega}\sin^2\theta, \quad (14a)$$

$$\delta n_y = -\gamma h_x \frac{\gamma(H_s+4\pi M_s) + i\omega\left[\alpha_0 + \frac{\alpha_n(1-\eta)}{1-\eta\cos 2\theta}\right]}{\omega^2 - \omega_{\rm A}^2 - i\Delta_{\rm A}\omega}\cos\theta\sin\theta, \quad (14b)$$

$$\delta m_z = -\gamma h_x \frac{i\omega}{\omega^2 - \omega_{\rm A}^2 - i\Delta_{\rm A}\omega}\sin\theta, \quad (14c)$$

$$\delta n_x = -\gamma h_y \frac{4\pi\gamma M_s + i\omega\left[\alpha_0 + \frac{\alpha_n(1-\eta)}{1+\eta\cos 2\theta}\right]}{\omega^2 - \omega_{\rm O}^2 - i\Delta_{\rm O}\omega}\cos\theta\sin\theta, \quad (15a)$$

$$\delta m_y = \gamma h_y \frac{4\pi\gamma M_s + i\omega\left[\alpha_0 + \frac{\alpha_m(1+\eta)}{1-\eta\cos 2\theta}\right]}{\omega^2 - \omega_{\rm O}^2 - i\Delta_{\rm O}\omega}\cos^2\theta, \quad (15b)$$

$$\delta n_z = \gamma h_y \frac{i\omega}{\omega^2 - \omega_{\rm O}^2 - i\Delta_{\rm O}\omega}\cos\theta. \quad (15c)$$

The A modes (δm_x,δn_y,δm_z) are excited by h_x, while the O modes (δn_x,δm_y,δn_z) couple to h_y. The poles in $\delta\mathbf{m}(\omega)$ and $\delta\mathbf{n}(\omega)$ define the resonance frequencies and linewidths that do not depend on the magnetic field since we disregard anisotropy and exchange bias.

A. Acoustic and optical modes

An antiferromagnetically exchange-coupled spin valve generally has noncollinear magnetization configurations by the presence of external magnetic fields. For $H < H_s$ ($0 < \theta < \pi/2$), the acoustic mode,

$$\omega_{\rm A} = \gamma H\sqrt{1 + (4\pi M_s/H_s)}, \quad (16)$$

$$\begin{aligned}\Delta_{\rm A} &= \alpha_0\gamma(H_s + 4\pi M_s + H_s\sin^2\theta)\\ &\quad + \alpha_m\gamma(H_s + 4\pi M_s) + \alpha_{\rm A}(\theta)\gamma H_s, \quad (17)\end{aligned}$$

and the optical mode,

$$\omega_{\rm O} = \gamma\sqrt{(4\pi M_s/H_s)\left(H_s^2 - H^2\right)}, \quad (18)$$

$$\begin{aligned}\Delta_{\rm O} &= \alpha_0\gamma(4\pi M_s + H_s\cos^2\theta)\\ &\quad + \alpha_n 4\pi\gamma M_s + \alpha_{\rm O}(\theta)\gamma H_s, \quad (19)\end{aligned}$$

where

$$\alpha_{\rm A}(\theta) = \frac{\alpha_1 g_r\sin^2\theta}{1 + g_r\tanh(d_{\rm N}/2\lambda) + 2g_r\sin^2\theta/\sinh(d_{\rm N}/\lambda)}, \quad (20)$$

$$\alpha_{\rm O}(\theta) = \frac{\alpha_1 g_r\cos^2\theta}{1 + g_r\tanh(d_{\rm N}/2\lambda) + 2g_r\cos^2\theta/\sinh(d_{\rm N}/\lambda)}. \quad (21)$$

The additional broadening in $\Delta_{\rm A}$ is proportional to α_m and $\alpha_{\rm A}$, while that in $\Delta_{\rm O}$ scales with α_n and $\alpha_{\rm O}$. Figure 2(a) shows α_m and α_n as a function of spacer layer thickness, indicating that α_n is always larger than α_m, and that α_n (α_m) strongly increases (decreases) with decreasing N layer

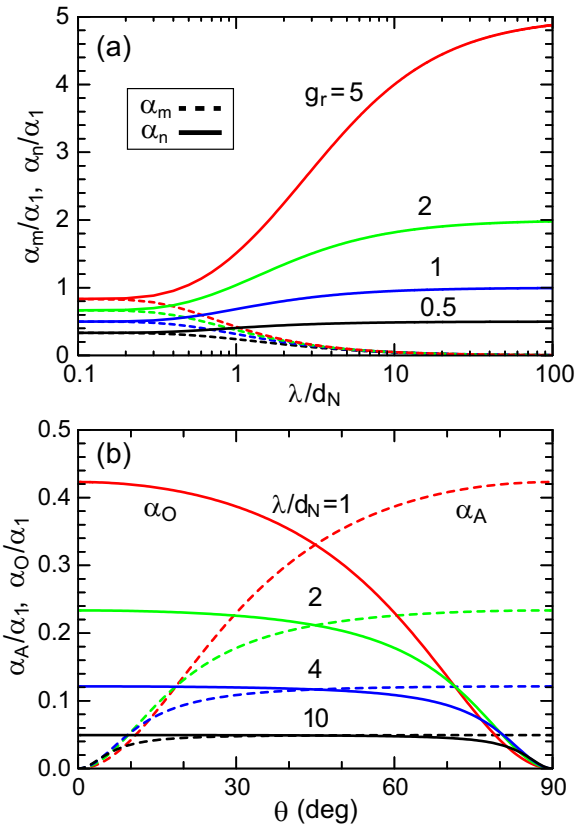

FIG. 2. (Color online) (a) α_m (dashed line) and α_n (solid line) as a function of $\lambda/d_{\rm N}$ for different values of the dimensionless mixing conductance g_r. (b) $\alpha_{\rm AC}$ (dashed line) and $\alpha_{\rm OP}$ (solid line) as a function of tilt angle θ for $g_r = 5$ and different values of $\lambda/d_{\rm N}$.

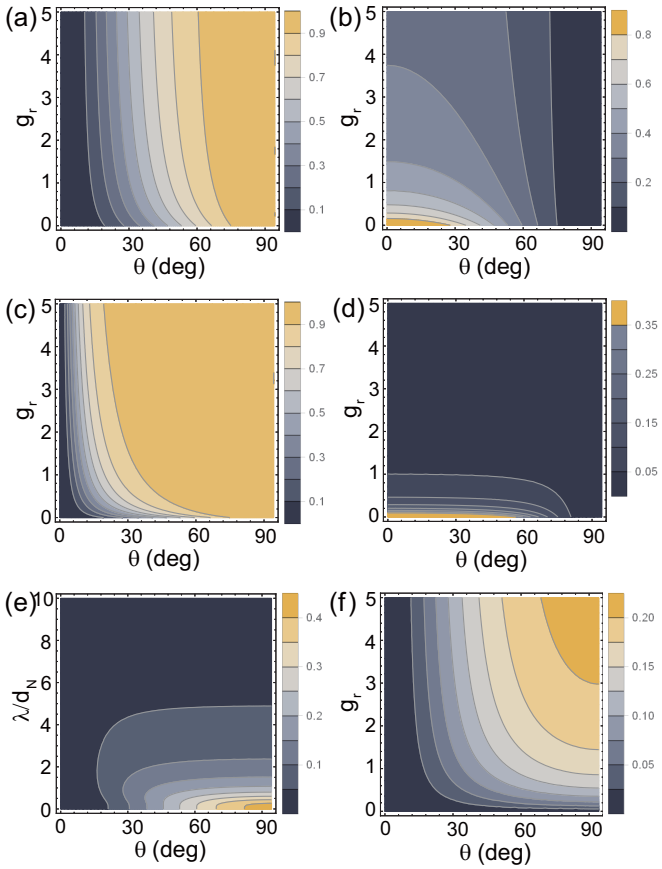

FIG. 3. (Color online) (a),(c) $\alpha_A(\theta)/\alpha_m$ and (b),(d) $\alpha_O(\theta)/\alpha_n$ as a function of θ and g_r for different values of λ/d_N. (a),(b) with $\lambda/d_N = 1$, (c),(d) with $\lambda/d_N = 10$, (e) $\alpha_A(\theta)/\alpha_0$ as a function of θ and λ/d_N with $g_r = 5$ and $\alpha_0 = 0.02$. (f) $\alpha_A(\theta)/\alpha_0$ as a function of θ and g_r with $\lambda/d_N = 1$ and $\alpha_0 = 0.02$.

thickness, especially for $d_N < \lambda$ and large g_r. Figure 2(b) shows the dependence of α_A and α_O on the tilted angle θ for different values of d_N. As θ increases, α_A increases from 0 to α_m while α_O decreases α_m to 0. The additional damping can be explained by the dynamic exchange. When two magnetizations in spin valves precess in phase, each magnet receives a spin current that compensates the pumped one, thereby reducing the interface damping. When the magnetizations precess out of phase, the π-phase difference between both spin currents means that the moduli have to be added, thereby enhancing the damping.

When the magnetizations are tilted by an angle θ, as sketched in Fig. 1, we predict an additional damping torque expressed by the second terms of Eqs. (4a) and (4b). Figure 3 shows the ratios $\alpha_A(\theta)/\alpha_m$ and $\alpha_O(\theta)/\alpha_n$ as a function of θ and g_r for different values of λ/d_N, thereby emphasizing the additional damping in the presence of noncollinear magnetizations. In Figs. 3(a) and 3(b), with $\lambda/d_N = 1$, i.e., for a spin-diffusive interlayer, the additional damping of both A and O modes is significant in a large region of parameter space. On the other hand, in Figs. 3(c) and 3(d), with $\lambda/d_N = 10$, i.e., for an almost spin-ballistic interlayer, the additional damping is more important for the A mode, while the O mode is affected only close to the collinear magnetization. In the latter case, the intrinsic damping α_0 dominates, however. Figures 3(e) and 3(f) show the ratios α_A/α_0 as a function of θ and g_r and λ/d_N, which allows valuating the importance of the noncollinear damping as compared to the angle-independent one. The O and A modes are related by $\alpha_O(\theta) = \alpha_A(\pi/2 - \theta)$.

B. In-phase and out-of-phase modes

When the applied magnetic field is larger than the saturation field ($H > H_s$), both magnetizations point in the $\hat{\mathbf{y}}$ direction, and the $\delta\mathbf{m}$ (A) and $\delta\mathbf{n}$ (O) modes change into in-phase and 180° out-of-phase (antiphase) oscillations of $\delta\mathbf{m}_1$ and $\delta\mathbf{m}_2$, respectively. The resonance frequency [55] and linewidth of the in-phase mode for $H > H_s$ ($\theta = \pi/2$) are

$$\omega_A = \gamma\sqrt{H(H + 4\pi M_s)}, \tag{22}$$

$$\Delta_A = 2(\alpha_0 + \alpha_m)\gamma(H + 2\pi M_s), \tag{23}$$

while those of the out-of-phase mode are

$$\omega_O = \gamma\sqrt{(H - H_s)(H - H_s + 4\pi M_s)}, \tag{24}$$

$$\Delta_O = 2(\alpha_0 + \alpha_n)\gamma(H - H_s + 2\pi M_s). \tag{25}$$

Figure 4(a) shows the calculated resonance frequencies of the A and O modes as a function of an applied magnetic

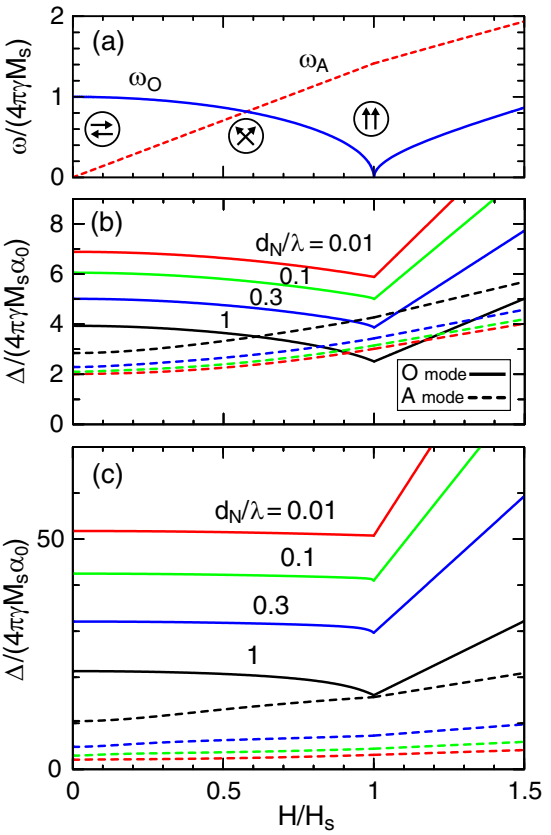

FIG. 4. (Color online) (a) Resonance frequencies of the A and O modes as a function of magnetic field for $H_s/(4\pi M_s) = 1$. (b),(c) Linewidths of the A (dashed line) and the O (solid line) modes for $H_s/(4\pi M_s) = 1$, $g_r = 5$, and different values of d_N/λ. (b) $\alpha_1/\alpha_0 = 1$ and (c) $\alpha_1/\alpha_0 = 10$.

field H, while Fig. 4(b) displays the linewidths for $\alpha_1/\alpha_0 = 1$, which is representative for ferromagnetic metals such as permalloy (Py) with an intrinsic magnetic damping of the order of $\alpha_0 = 0.01$ and a comparable additional damping α_1 due to spin pumping. A value $g_r = 4/5$ corresponds to $\lambda = 20/200$ nm, $\rho = 10/2.5\ \mu\Omega$cm for $N =$ Ru/Cu [56,57], $G_r = 2/1 \times 10^{15}\ \Omega^{-1}\mathrm{m}^{-2}$ for the N|Co (Py) interface [58,59], and $d_F = 1$ nm, for example. The colors in the figure represent different relative layer thicknesses d_N/λ. The linewidth of the A mode in Fig. 4(b) increases with increasing H, while that of the O mode starts to decrease until a minimum at the saturation field $H = H_s$. Figure 4(c) shows the linewidths for $\alpha_1/\alpha_0 = 10$, which describes ferromagnetic materials with low intrinsic damping, such as Heusler alloys [60] and magnetic garnets [61]. In this case, the linewidth of the O mode is much larger than that of the A mode, especially for small d_N/λ.

In the limit of $d_N/\lambda \to 0$, the expressions of the linewidth in Eqs. (17) and (19) are then greatly simplified to $\Delta_A = \gamma(H_s + 4\pi M_s + H_s \sin^2\theta)\alpha_0$ and $\Delta_O = \gamma(4\pi M_s + H_s\cos^2\theta)\alpha_0 + (4\pi\gamma M_s)g_r\alpha_1$, and $\Delta_A \ll \Delta_O$ when $g_r\alpha_1 \gg \alpha_0$. The additional damping, given by Eq. (10b), reduces to $\alpha_m \to 0$ and $\alpha_n \to 2[\gamma\hbar/(4\pi M_s d_F)(h/e^2)G_r]$ when the magnetizations are collinear and in the ballistic spin transport limit [27]. In contrast to the acoustic mode, the dynamic exchange interaction enhances damping of the optical mode. $\Delta_O \gg \Delta_A$ has been observed in Py|Ru|Py trilayer spin valves [32] and Co|Cu multilayers [30], consistent with the present results.

For spin valves with ferromagnetic metals, the interface backflow spin current [Eq. (1b)] reads $\mathbf{J}_j^B = (G_r/e)[\xi_F(\mathbf{m}_j\cdot\boldsymbol{\mu}_{sj})\mathbf{m}_j - \boldsymbol{\mu}_{sj}]$, where $\xi_F = 1 - (G/2G_r)(1-p^2)(1-\eta_F)$ $(0 \leqslant \xi_F \leqslant 1)$, G is the N | F interface conductance per unit area, and p is the conductance spin polarization [53]. Here the spin-diffusion efficiency is

$$\frac{1}{\eta_F} = 1 + \frac{\sigma_F}{G\lambda_F}\frac{\tanh(d_F/\lambda_F)}{\cosh(d_F/\lambda_F)}, \tag{26}$$

where σ_F, λ_F, and d_F are the conductivity, the spin-flip diffusion length, and the layer thickness of the ferromagnets, respectively. For the material parameters of a typical ferromagnet with $d_F = 1$ nm, the resistivity $\rho_F = 10\ \mu\Omega$ cm, $G = 2G_r = 10^{15}\ \Omega^{-1}\,\mathrm{m}^{-2}$, $\lambda_F = 10$ nm, and $p = 0.7$, $\xi_F = 0.95$, which justifies disregarding this contribution from the outset.

V. COMPARISON WITH EXPERIMENTS

FMR experiments measure the resonant absorption spectrum of a microwave field by a ferromagnet. The microwave absorption power $P = 2\langle\mathbf{h}(t)\cdot\partial_t\mathbf{m}(t)\rangle$ becomes, in our model,

$$P = \frac{1}{4}\frac{\gamma^2 M_s(H_s+4\pi M_s)\Delta_A}{(\omega-\omega_A)^2+(\Delta_A/2)^2}h_x^2\sin^2\theta + \frac{1}{4}\frac{\gamma^2 M_s(4\pi M_s)\Delta_O}{(\omega-\omega_O)^2+(\Delta_O/2)^2}h_y^2\cos^2\theta. \tag{27}$$

P depends sensitively on the character of the resonance, the polarization of the microwave, and the strength of the applied magnetic field. In Fig. 5(a), we plot the normalized derivative of the microwave absorption spectra $dP/(P_0 dH)$ at different angles φ between the microwave field $\mathbf{h}(t)$ and the external magnetic field $\mathbf{H}$, where $P_0 = \gamma M_s h^2$ and $\mathbf{h}(t) = h(\sin\varphi, \cos\varphi, 0)e^{i\omega t}$. Here we use the experimental values $H_s = 5$ kOe, $4\pi M_s = 10$ kOe, $d_N = 1$ nm, $d_F = 3$ nm, and microwave frequency $\omega/(2\pi) = 9.22$ GHz as found for a symmetric Co|Ru|Co trilayer [31]. $\lambda = 20$ nm for Ru, $\alpha_0 = \alpha_1 = 0.02$, and $g_r = 4$ is adopted (corresponding to $G_r = 2\times 10^{15}\ \Omega^{-1}\,\mathrm{m}^{-2}$). When $\mathbf{h}(t)$ is perpendicular to $\mathbf{H}$ ($\varphi = 90^\circ$), only the A mode is excited by the transverse $(\delta m_x, \delta m_z)$ component. When $\mathbf{h}(t)$ is parallel to $\mathbf{H}$ ($\varphi = 0^\circ$), the O mode couples to the microwave field by the longitudinal δm_y component. For intermediate angles ($\varphi = 20^\circ$), both modes are excited at resonance. We observe that the optical mode signal is broader than the acoustic one, as calculated. The theoretical resonance linewidths of the A and O modes as well as the absorption power as a function of microwave polarization reproduce the experimental results for Co(3.2 nm)|Ru(0.95 nm)|Co(3.2 nm) well [31].

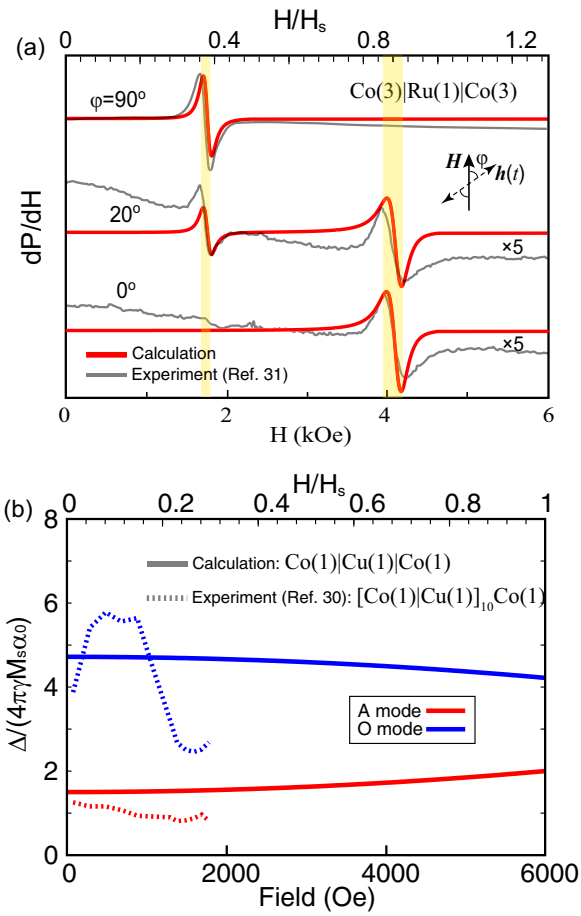

FIG. 5. (Color online) (a) Derivative of the microwave absorption spectrum dP/dH at frequency $\omega/(2\pi) = 9.22$ GHz for different angles φ between the microwave field and the external magnetic field for $H_s/(4\pi M_s) = 0.5$, $\omega/(4\pi\gamma M_s) = 0.35$, $d_N/\lambda = 0.1$, $d_F/\lambda = 0.3$, $\alpha_0 = \alpha_1 = 0.02$, and $g_r = 4$. The experimental data have been adopted from Ref. [31]. (b) Computed linewidths of the A and O modes of a Co|Cu|Co spin valve (solid line) compared with experiments on a Co|Cu multilayer (dashed line) [30].

Figure 5(b) shows the calculated linewidths of the A and O modes as a function of an applied magnetic field for a Co(1 nm)|Cu(1 nm)|Co(1 nm) spin valve. The experimental

values $\lambda = 200$ nm and $\rho = 2.5\ \mu\Omega$ cm for Cu, $\alpha_0 = 0.01$ and $4\pi M_s = 15$ kOe for Co, and $g_r = 5$ (corresponding to $G_r = 10^{15}\ \Omega^{-1}\,\mathrm{m}^{-2}$) for the interface have been adopted [59]. We find agreement for the zero-field broadenings for magnetic multilayers, but the field dependence is not reproduced very well, which is not so surprising considering the different type of samples. The increased/decreased broadening of acoustic/optic modes can be explained by the mutual pumping of spin currents. Equations (17) and (19) are dominated by the intrinsic damping, i.e., the field-dependent contribution to Eqs. (20) and (21) is small for these parameters. The small but rapid changes observed under an applied magnetic field might reflect exchange-dipolar [43] and/or multilayer [30] spin waves beyond our spin-valve macrospin model.

VI. CONCLUSIONS

In summary, we modeled the magnetization dynamics in antiferromagnetically exchange-coupled spin valves as a model for synthetic antiferromagnets. We derive the Landau-Lifshitz-Gilbert equations for the coupled magnetizations including the spin-transfer torques by spin pumping based on the spin-diffusion model with quantum mechanical boundary conditions. We obtain analytic expressions for the linewidths of magnetic resonance modes for magnetizations canted by applied magnetic fields and achieve favorable agreement with experiments. We find that the linewidths strongly depend on the type of resonance mode (acoustic and optical) as well as the strength of magnetic fields. The magnetic resonance spectra reveal complex magnetization dynamics far beyond a simple precession, even in the linear response regime. Our calculated results compare favorably with the limited number of experiments, thereby proving the importance of dynamic spin currents in these devices. Our model calculation paves the way for the theoretical design of synthetic AFM material that is expected to play a role in next-generation spin-based data-storage and information technologies.

ACKNOWLEDGMENTS

The authors thanks K. Tanaka, T. Moriyama, T. Ono, T. Yamamoto, T. Seki, and K. Takanashi for valuable discussions and collaborations. This work was supported by Grants-in-Aid for Scientific Research (Grants No. 22540346, No. 25247056, No. 25220910, and No. 268063) from the JSPS, FOM (Stichting voor Fundamenteel Onderzoek der Materie), the ICC-IMR, EU-FET Grant InSpin No. 612759, and DFG Priority Programme 1538 "Spin-Caloric Transport" (BA 2954/2).

APPENDIX: COUPLED LANDAU-LIFSHITZ-GILBERT EQUATIONS IN NONCOLLINEAR SPIN VALVES

Both magnets and interfaces in our NM|F|NM spin valves are assumed to be identical to saturation magnetization M_s and G_r, which is the real part of the spin-mixing conductance per unit area (vanishing imaginary part). When both magnetizations are allowed to precess, as sketched in Fig. 1(a), the LLG equations that are expanded to include additional spin-pump and spin-transfer torques read

$$\frac{\partial \mathbf{m}_i}{\partial t} = -\gamma \mathbf{m}_i \times \mathbf{H}_{\mathrm{eff}i} + \alpha_{0i}\mathbf{m}_i \times \frac{\partial \mathbf{m}_i}{\partial t} + \alpha_{\mathrm{SP}i}\left[\mathbf{m}_i \times \frac{\partial \mathbf{m}_i}{\partial t} - \eta \mathbf{m}_j \times \frac{\partial \mathbf{m}_j}{\partial t} + \eta\left(\mathbf{m}_i \cdot \mathbf{m}_j \times \frac{\partial \mathbf{m}_j}{\partial t}\right)\mathbf{m}_i\right] + \tau^{\mathrm{nc}}_{\mathrm{SP}i}(\psi)\mathbf{m}_i \times (\mathbf{m}_i \times \mathbf{m}_j), \tag{A1}$$

$$\tau^{\mathrm{nc}}_{\mathrm{SP}i}(\psi) = \frac{\alpha_{\mathrm{SP}i}\eta^2}{1-\eta^2(\mathbf{m}_i \cdot \mathbf{m}_j)^2}\left[\mathbf{m}_j \cdot \mathbf{m}_i \times \frac{\partial \mathbf{m}_i}{\partial t} + \eta(\mathbf{m}_j \cdot \mathbf{m}_i)\left(\mathbf{m}_i \cdot \mathbf{m}_j \times \frac{\partial \mathbf{m}_j}{\partial t}\right)\right], \tag{A2}$$

where γ and α_{0i} are the gyromagnetic ratio and the Gilbert damping constant of the isolated ferromagnetic films labeled by i and thickness $d_{\mathrm{F}i}$. Asymmetric spin valves due to the thickness difference $d_{\mathrm{F}i}$ suppress the cancellation of mutual spin pump in the A mode, which may be an advantage to detect both modes in the experiment. The effective magnetic field in layer i,

$$\mathbf{H}_{\mathrm{eff}i} = \mathbf{H}_i + \mathbf{h}(t) + \mathbf{H}_{\mathrm{di}i}(t) + \mathbf{H}_{\mathrm{ex}j}(t), \tag{A3}$$

consists of the Zeeman field $\mathbf{H}_i$, a microwave field $\mathbf{h}(t)$, the dynamic demagnetization field $\mathbf{H}_{\mathrm{di}i}(t)$, and interlayer exchange field $\mathbf{H}_{\mathrm{ex}j}(t)$. The Gilbert damping torque parameterized by α_{0i} governs the relaxation towards an equilibrium direction. The third term in Eq. (A1) represents the mutual spin-pumping-induced dampinglike torques in terms of damping parameter,

$$\alpha_{\mathrm{SP}i} = \frac{\gamma\hbar^2 G_r}{2e^2 M_s d_{\mathrm{F}i}}\frac{\eta S}{1-\eta^2}, \tag{A4}$$

where

$$\eta = \frac{g_r}{\sinh(d_{\mathrm{N}}/\lambda) + g_r \cosh(d_{\mathrm{N}}/\lambda)} \tag{A5}$$

and $g_r = 2\lambda\rho G_r$ is dimensionless. The fourth term in Eq. (A1) is the damping torque given by Eq. (A2) that depends on the relative angle ψ between the magnetizations. When $\mathbf{m}_j$ is fixed along the $\mathbf{H}_i$ direction, i.e., a spin-sink limit, Eq. (A1) reduces to the dynamic stiffness in spin valves without an electrical bias [62].

When the magnetizations are noncollinear as in Fig. 1, we have to take into account the additional damping torques described by the second terms in Eqs. (4a) and (4b). In the ballistic limit $d_{\mathrm{N}}/\lambda \to 0$ and collinear magnetizations, Eq. (A1) reduces to the well-known LLG equation with dynamic exchange coupling [27,28,40].

[1] X. Marti, I. Fina, C. Frontera, Jian Liu, P. Wadley, Q. He, R. J. Paull, J. D. Clarkson, J. Kudrnovský, I. Turek, J. Kuneš, D. Yi, J-H. Chu, C. T. Nelson, L. You, E. Arenholz, S. Salahuddin, J. Fontcuberta, T. Jungwirth, and R. Ramesh, Nat. Mater. **13**, 367 (2014).

[2] B. G. Park, J. Wunderlich, X. Martí, V. Holý, Y. Kurosaki, M. Yamada, H. Yamamoto, A. Nishide, J. Hayakawa, H. Takahashi, A. B. Shick, and T. Jungwirth, Nat. Mater. **10**, 347 (2011).

[3] P. M. Haney, D. Waldron, R. A. Duine, A. S. Núnez, H. Guo, and A. H. MacDonald, Phys. Rev. B **75**, 174428 (2007).

[4] Z. Wei, A. Sharma, A. S. Nunez, P. M. Haney, R. A. Duine, J. Bass, A. H. MacDonald, and M. Tsoi, Phys. Rev. Lett. **98**, 116603 (2007).

[5] S. Urazhdin and N. Anthony, Phys. Rev. Lett. **99**, 046602 (2007).

[6] Y. Xu, S. Wang, and K. Xia, Phys. Rev. Lett. **100**, 226602 (2008).

[7] K. M. D. Hals, Y. Tserkovnyak, and A. Brataas, Phys. Rev. Lett. **106**, 107206 (2011).

[8] H. V. Gomonay, R. V. Kunitsyn, and V. M. Loktev, Phys. Rev. B **85**, 134446 (2012).

[9] C. Hahn, G. de Loubens, V. V. Naletov, J. B. Youssef, O. Klein, and M. Viret, Eur. Phys. Lett. **108**, 57005 (2014).

[10] H. Wang, C. Du, P. C. Hammel, and F. Yang, Phys. Rev. Lett. **113**, 097202 (2014).

[11] T. Moriyama, S. Takei, M. Nagata, Y. Yoshimura, N. Matsuzaki, T. Terashima, Y. Tserkovnyak, and T. Ono, Appl. Phys. Lett. **106**, 162406 (2015).

[12] R. Duine, Nat. Mater. **10**, 344 (2011).

[13] A. H. MacDonald and M. Tsoi, Phil. Trans. R. Soc. A **369**, 3098 (2011).

[14] A. V. Kimel, A. Kirilyuk, P. A. Usachev, R. V. Pisarev, A. M. Balbashov, and Th. Rasing, Nature (London) **435**, 655 (2005).

[15] T. Satoh, S.-J. Cho, R. Iida, T. Shimura, K. Kuroda, H. Ueda, Y. Ueda, B. A. Ivanov, F. Nori, and M. Fiebig, Phys. Rev. Lett. **105**, 077402 (2010).

[16] S. Wienholdt, D. Hinzke, and U. Nowak, Phys. Rev. Lett. **108**, 247207 (2012).

[17] P. Grünberg, R. Schreiber, Y. Pang, M. B. Brodsky, and H. Sowers, Phys. Rev. Lett. **57**, 2442 (1986).

[18] P. Grünberg, D. E. Bürgler, H. Dassow, A. D. Rata, and C. M. Schneider, Acta Mater. **55**, 1171 (2007).

[19] S. S. P. Parkin, X. Jiang, C. Kaiser, A. Panchula, K. Roche, and M. Samant, Proc. IEEE **91**, 661 (2003).

[20] M. N. Baibich, J. M. Broto, A. Fert, F. Nguyen Van Dau, F. Petroff, P. Etienne, G. Creuzet, A. Friederich, and J. Chazelas, Phys. Rev. Lett. **61**, 2472 (1988).

[21] G. Binasch, P. Grünberg, F. Saurenbach, and W. Zinn, Phys. Rev. B **39**, 4828 (1989).

[22] A. Brataas, A. D. Kent, and H. Ohno, Nat. Mater. **11**, 372 (2012).

[23] E. Chen, D. Apalkov, Z. Diao, A. Driskill-Smith, D. Druist, D. Lottis, V. Nikitin, X. Tang, S. Watts, S. Wang, S. Wolf, A. W. Ghosh, J. Lu, S. J. Poon, M. Stan, W. Butler, S. Gupta, C. K. A. Mewes, T. Mewes, and P. Visscher, IEEE Trans. Magn. **46**, 1873 (2010).

[24] D. C. Ralph and M. D. Stiles, J. Magn. Magn. Mater. **320**, 1190 (2008).

[25] M. J. Carey, N. Smith, S. Maat, and J. R. Childress, Appl. Phys. Lett. **93**, 102509 (2008).

[26] Y. Tserkovnyak, A. Brataas, and G. E. W. Bauer, Phys. Rev. Lett **88**, 117601 (2002).

[27] Y. Tserkovnyak, A. Brataas, G. E. W. Bauer, and B. I. Halperin, Rev. Mod. Phys. **77**, 1375 (2005).

[28] B. Heinrich, Y. Tserkovnyak, G. Woltersdorf, A. Brataas, R. Urban, and G. E. W. Bauer, Phys. Rev. Lett. **90**, 187601 (2003).

[29] S. Takahashi, Appl. Phys. Lett. **104**, 052407 (2014).

[30] K. Tanaka, T. Moriyama, M. Nagata, T. Seki, K. Takanashi, S. Takahashi, and T. Ono, Appl. Phys. Express **7**, 063010 (2014).

[31] Z. Zhang, L. Zhou, P. E. Wigen, and K. Ounadjela, Phys. Rev. Lett. **73**, 336 (1994).

[32] M. Belmeguenai, T. Martin, G. Woltersdorf, M. Maier, and G. Bayreuther, Phys. Rev. B **76**, 104414 (2007).

[33] R. L. Stamps, Phys. Rev. B **49**, 339 (1994).

[34] X. Joyeux, T. Devolder, J.-V. Kim, Y. G. de la Torre, S. Eimer, and C. Chappert, J. Appl. Phys. **110**, 063915 (2011).

[35] H. Skarsvåg, G. E. W. Bauer, and A. Brataas, Phys. Rev. B **90**, 054401 (2014).

[36] Pavel Baláž and Józef Barnaś, Phys. Rev. B **91**, 104415 (2015).

[37] S. O. Demokritov, B. Hillebrands, and A. N. Slavin, Phys. Rep. **348**, 441 (2001).

[38] J. F. Cochran, J. Rudd, W. B. Muir, B. Heinrich, and Z. Celinski, Phys. Rev. B **42**, 508 (1990).

[39] B. K. Kuanr, M. Buchmeier, D. E. Bürgler, and P. Grünberg, J. Appl. Phys. **91**, 7209 (2002).

[40] A. A. Timopheev, Yu. G. Pogorelov, S. Cardoso, P. P. Freitas, G. N. Kakazei, and N. A. Sobolev, Phys. Rev. B **89**, 144410 (2014).

[41] T. Taniguchi and H. Imamura, Phys. Rev. B **76**, 092402 (2007).

[42] J.-V. Kim and C. Chappert, J. Magn. Magn. Mater. **286**, 56 (2005).

[43] H. Skarsvåg, André Kapelrud, and A. Brataas, Phys. Rev. B **90**, 094418 (2014).

[44] Y. Zhou, J. Xiao, G. E. W. Bauer, and F. C. Zhang, Phys. Rev. B **87**, 020409(R) (2013).

[45] A. Layadi and J. O. Artman, J. Magn. Magn. Mater. **176**, 175 (1997).

[46] B. K. Kuanr, M. Buchmeier, R. R. Gareev, D. E. Bürgler, R. Schreiber, and P. Grünberg, J. Appl. Phys. **93**, 3427 (2003).

[47] R. F. L. Evans, T. A. Ostler, R. W. Chantrell, I. Radu, and T. Rasing, Appl. Phys. Lett. **104**, 082410 (2014).

[48] D. E. Gonzalez-Chavez, R. Dutra, W. O. Rosa, T. L. Marcondes, A. Mello, and R. L. Sommer, Phys. Rev. B **88**, 104431 (2013).

[49] X. M. Liu, Hoa T. Nguyen, J. Ding, M. G. Cottam, and A. O. Adeyeye, Phys. Rev. B **90**, 064428 (2014).

[50] J. J. Krebs, P. Lubitz, A. Chaiken, and G. A. Prinz, J. Appl. Phys. **67**, 5920 (1990).

[51] T. Chiba, G. E. W. Bauer, and S. Takahashi, Phys. Rev. Appl. **2**, 034003 (2014).

[52] T. Chiba, M. Schreier, G. E. W. Bauer, and S. Takahashi, J. Appl. Phys. **117**, 17C715 (2015).

[53] H. J. Jiao and G. E. W. Bauer, Phys. Rev. Lett. **110**, 217602 (2013).

[54] X. Jia, K. Liu, K. Xia, and G. E. W. Bauer, Europhys. Lett. **96**, 17005 (2011).

[55] Z. Zhang and P. E. Wigen, *High Frequency Processes in Magnetic Materials*, edited by G. Srinivasan and A. N. Slavin (World Scientific, Singapore, 1995).

[56] K. Eid, R. Fonck, M. AlHaj Darwish, W. P. Pratt Jr., and J. Bass, J. Appl. Phys. **91**, 8102 (2002).

[57] S. Yakata, Y. Ando, T. Miyazaki, and S. Mizukami, Jpn. J. Appl. Phys. **45**, 3892 (2006).
[58] X. Jia, Y. Li, K. Xia, and G. E. W. Bauer, Phys. Rev. B **84**, 134403 (2011).
[59] K. Xia, P. J. Kelly, G. E. W. Bauer, A. Brataas, and I. Turek, Phys. Rev. B **65**, 220401 (2002).
[60] S. Mizukami, D. Watanabe, M. Oogane, Y. Ando, Y. Miura, M. Shirai, and T. Miyazaki, J. Appl. Phys. **105**, 07D306 (2009).
[61] J. M. D. Coey, *Magnetism and Magnetic Materials* (Cambridge University Press, Cambridge, 2010).
[62] Y. Tserkovnyak, A. Brataas, and G. E. W. Bauer, Phys. Rev. B **67**(R), 140404 (2003)